Chapter 3
Nano-additives for development of Castor oil and Engine oil-based Nanofluids

The four distinct nano-additives were chosen to develop castor oil (CO) and engine oil (EO)-based nanofluids for their improved flow & thermal behaviour. These nano-additives, namely alumina (Al_2O_3) [1-4], zinc oxide (ZnO) [5-8], graphene nanoplatelets (GNP) [9-12], and multiwalled carbon nanotubes (MWCNT) [13-16], represent a diverse spectrum of nano materials with promising potential to enhance the flow characteristics and thermal conductivity of selected base oils [17-19].

This chapter covered the hydrothermal synthesis of the two metal-oxide nano-additives, namely Al_2O_3, and ZnO along with their systematic characterization using various techniques such as X-ray Diffraction (XRD), Scanning Electron Microscopy (SEM), and Energy Dispersive X-ray Spectroscopy (EDX). Furthermore, the chapter also furnished the data of commercially available carbon-based nano-additives i.e., GNP and MWCNT. Here, these carbon-based nano-additives were also properly characterized to understand their structures and morphologies for their further use.

3.1: Alumina (Al_2O_3) nanoparticles

3.1.1: Synthesis of Al_2O_3 nanoparticles using hydrothermal technique

To begin the synthesis process, 20 mL of 0.05M aluminium chloride, $AlCl_3$. $6H_2O$ and 20 mL of 1.0 M NaOH aqueous solution were mixed. To adjust the pH to 12, an aq. NaOH solution was added to the solution of $AlCl_3$. $6H_2O$ with constantly stirring.

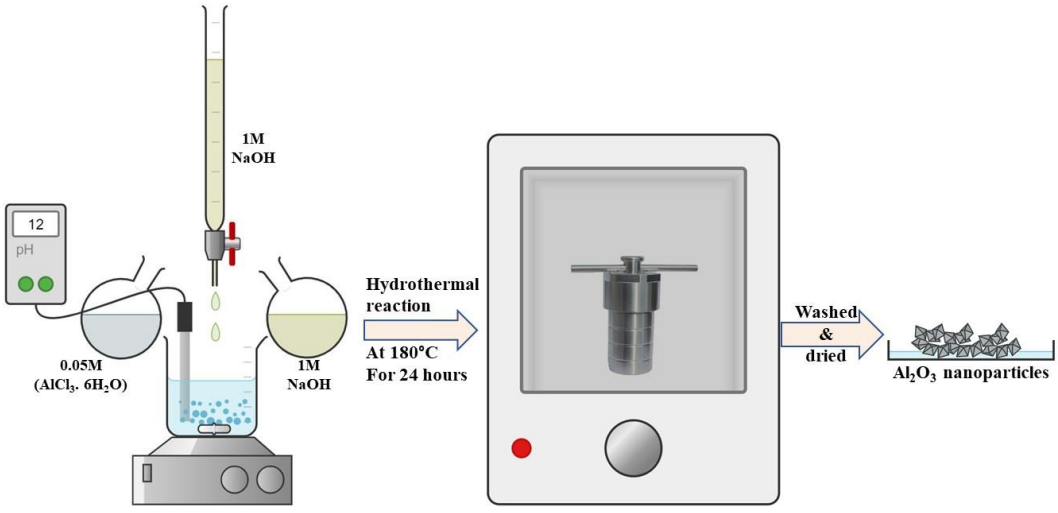

Fig. 3.1: Schematic illustration of synthesis of Al_2O_3 nanoparticles by hydrothermal method.

Initially, adding the NaOH solution, $Al(OH)_3$ white precipitate was produced which is then dissolved with the sufficient amount of NaOH solution and the solution turns transparent.

The resulting solutions were transferred to a PTFE closing arrangement and sealed in high quality non-magnetic 316 stainless steel (SS) hydrothermal reactor. The hydrothermal reactor heated at 180°C for 24 hours. After 24 hours, the reactor was allowed to cool at ambient temperatures. The powder form of Al_2O_3 nanoparticles is obtained, which was properly washed and dried for further characterization [20]. The entire process is illustrated in Fig. 3.1.

3.1.2: Characterization of Al_2O_3 nanoparticles

The XRD patterns of Al_2O_3 nanoparticles were shown in Fig. 3.2. It shows major diffraction peaks at $2\theta = 35.1°$, 43.2° and 57.4°, corresponding to the (104), (113) and (116) reflections, respectively. All the peaks of Al_2O_3 nanoparticles can be indexed to the rhombo hydral crystal system Al_2O_3 (R-3c space group, PDF 00-011-0661) [21]. Absence of impurities XRD peaks indicates that high quality of Al_2O_3 nanoparticles was prepared. The crystallite size was determined from XRD using the Scherrer's equation [22]. The crystallite size of highest peak in XRD was 69.59 nm < 100nm. It suggested nanocrystalline characteristic of Al_2O_3 nanoparticles. The lattice parameters of Al_2O_3 nanoparticles are also reported in Table 3.1.

Table 3.1: The lattice parameters of Al_2O_3 nanoparticles.

Nano-additive	**Lattice parameters**		**Full width at half maximum-FWHM (2θ) at peak 2θ=35.1°**	**Crystallite size by XRD (nm)**
	a	*c*		
Al_2O_3 nanoparticles	4.75	12.99	0.125°	69.59

Structure and morphological features of different Al_2O_3 samples were examined by SEM and the corresponding images are presented. Fig 3.3 shows hydrothermally synthesized Al_2O_3 additive have nano sized particles of less than 100 nm size. The composition of the Al_2O_3 nano-additive was determined from different regions using EDX spectroscopy. The corresponding EDX spectra (Fig 3.4) peaks showed Al, and O elements. Not having another peak suggested that hydrothermally synthesized Al_2O_3 nano-additive is free from impurities. It contained 44.38 wt.% Al, and 55.62 wt.% O. The morphology and EDX analysis were in support of the XRD results which confirm the purity of Al_2O_3 nano-additive.

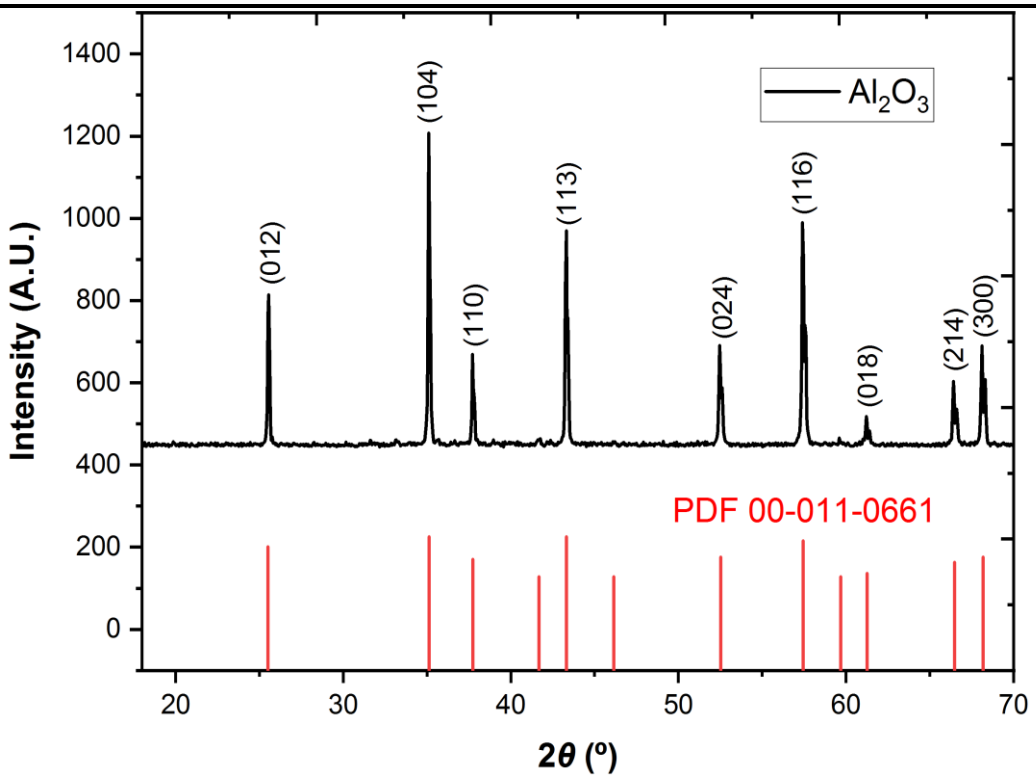

Fig. 3.2: XRD patterns of Al_2O_3 nanoparticles.

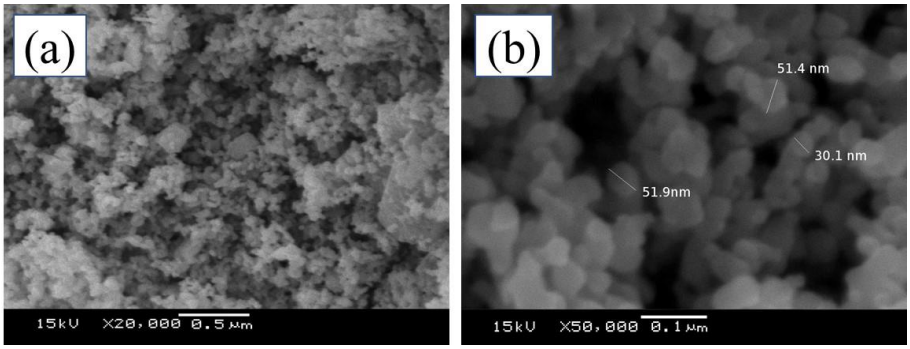

Fig. 3.3: SEM images of Al_2O_3 nanoparticles.

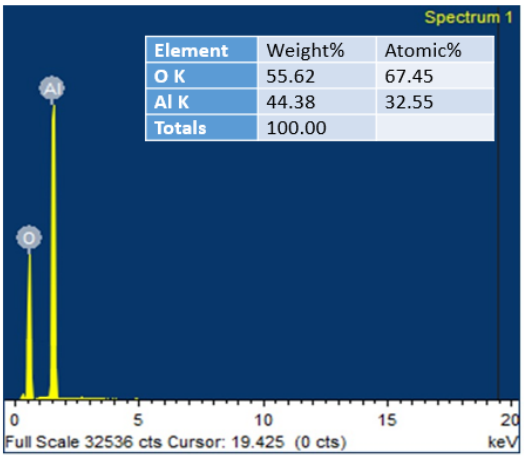

Fig. 3.4: EDX images of Al_2O_3 nanoparticles.

3.2: Zinc oxide (ZnO) nanoparticles

3.2.1: Synthesis of ZnO nanoparticles using hydrothermal technique

To begin the synthesis process, 20 mL of 0.05M zinc acetate, $Zn(CH_3COO)_2 \cdot 2H_2O$ and 20 mL of aqueous 1.0 M NaOH solution were mixed. To maintain the pH 12, the aq. NaOH solution was added to solution of zinc acetate, $Zn(CH_3COO)_2 \cdot 2H_2O$ with continuous stirring. Initially, by adding the base solution, the white precipitate of $Zn(OH)_2$ was produced. After adding a sufficient amount of NaOH solution, the precipitates is dissolved in the solution and it turns transparent containing $Zn(OH)_4^{2-}$ growth units. The resulting solutions were transferred to a closed PTFE arrangement and sealed in high quality non-magnetic 316 stainless steel (SS) hydrothermal reactor. The hydrothermal reactor heated at 180°C for 24 hours. After 24 hours, the reactor was allowed to cool at ambient temperatures. The powder form of ZnO nanoparticles is obtained, which was properly washed & dried for further characterization [23]. The entire process is illustrated in Fig. 3.5.

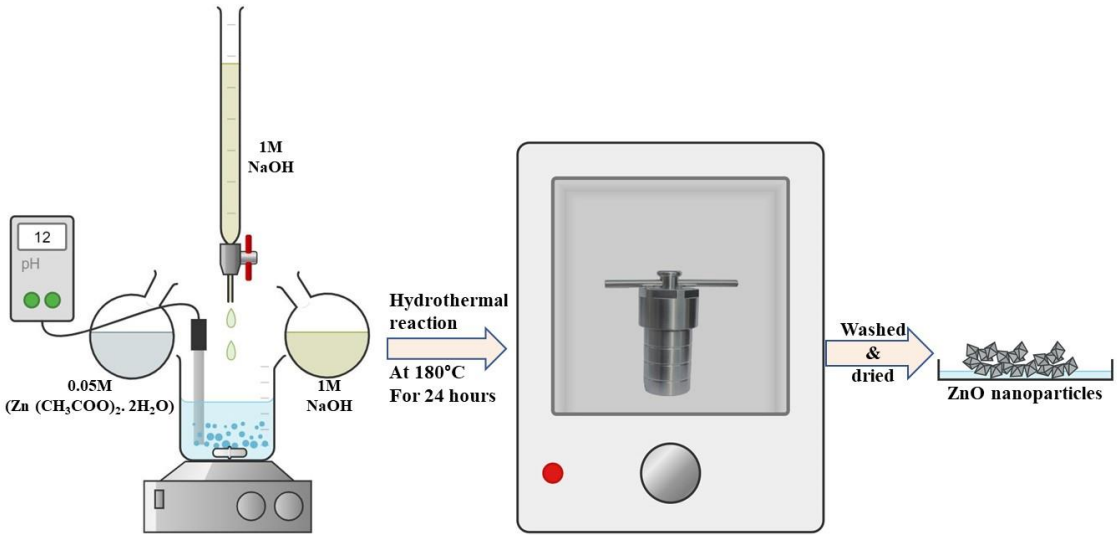

Fig. 3.5: Schematic illustration of synthesis of ZnO nanoparticles by hydrothermal method.

3.2.2: Characterization of ZnO nanoparticles

The XRD patterns of ZnO nanoparticles were shown in Fig. 3.6. It shows major diffraction peaks at 2θ = 31.8°, 34.4° and 36.3°, corresponding to the (100), (002) and (101) reflections, respectively. All the peaks of ZnO nanoparticles can be indexed to the hexagonal crystal system ZnO (P63mc space group, PDF 01-070-8070) [24]. Absence of impurities XRD peaks indicates that high quality of ZnO nanoparticles was prepared.

The crystallite size of highest peak in XRD was 44.31 nm < 100nm. It suggested nanocrystalline characteristic of ZnO nanoparticles. The lattice parameters of ZnO nanoparticles obtained through XRD analysis are also reported in Table 3.2.

Table 3.2: The lattice parameters of ZnO nanoparticles.

Nano-additive	Lattice parameters		Full width at half maximum-FWHM (2θ) at peak 2θ=36.3°	Crystallite size (nm)
	a	*c*		
ZnO nanoparticles	3.25	5.20	0.197°	44.31

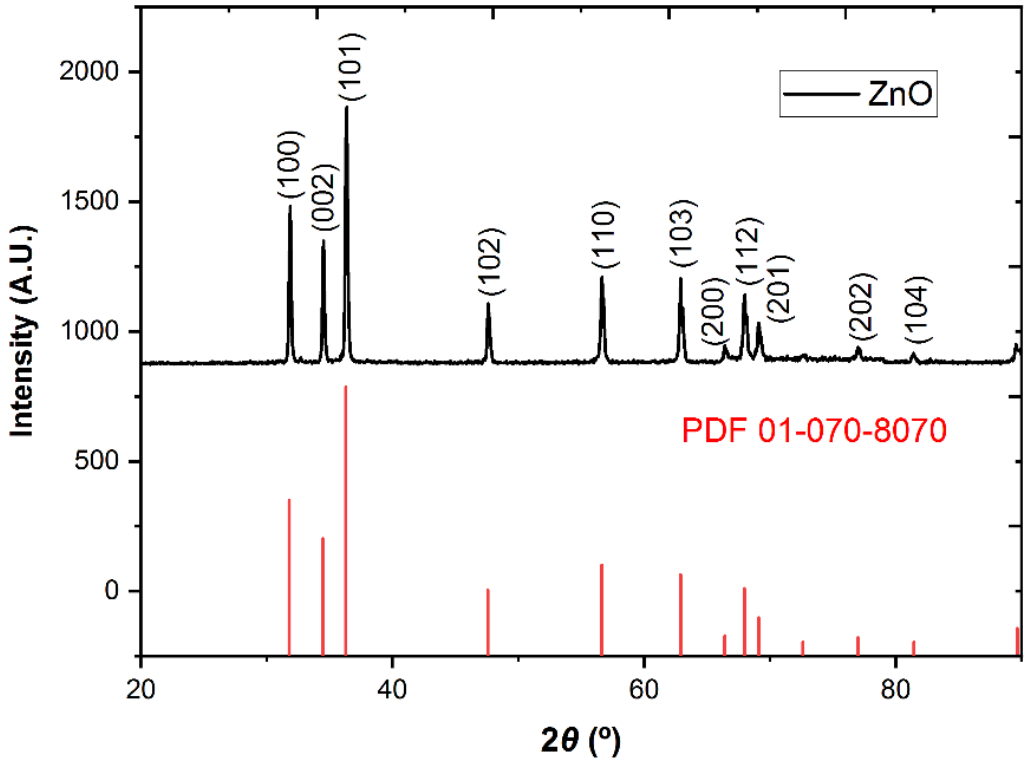

Fig. 3.6: XRD patterns of ZnO nanoparticles.

Structure and morphological features of ZnO samples were examined by SEM and the corresponding images are presented in the Fig 3.7. The images clearly show hydrothermally synthesized ZnO additive have nano sized particles of less than 100 nm size. The composition of the ZnO nano-additive was determined from different regions using EDX spectroscopy. The corresponding EDX spectra (Fig 3.8) peaks showed the presence of Zn, and O. Not having another peak suggests that the hydrothermally synthesized ZnO nano-additive is free from impurities. It contained 74.94 wt.% Zn, and

25.06 wt.% O. The morphology and EDX analysis were found in support with the XRD results which confirm the purity of ZnO nano-additive.

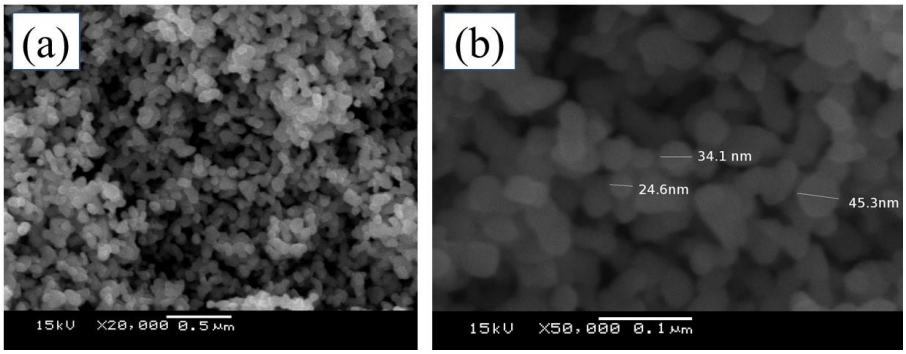

Fig. 3.7: SEM images of ZnO nanoparticles.

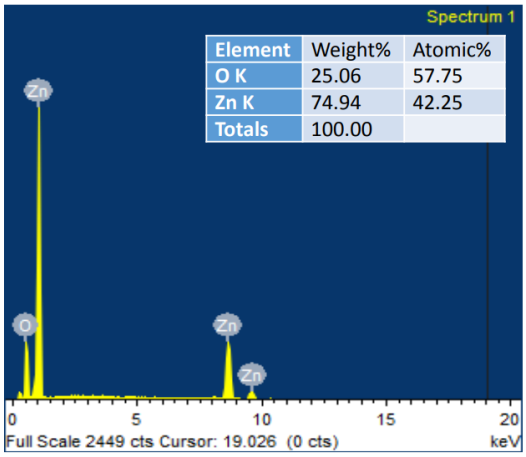

Fig. 3.8: EDX images of ZnO nanoparticles.

3.3: Graphene nanoplatelets (GNP)

Graphene nanoplatelets (GNP) was acquired from Sigma-Aldrich (USA) and utilized without additional purification.

3.3.1: Characterization of GNP nanoparticles

The XRD graph of GNP nano-additives exhibits characteristic peaks (Fig. 3.9) indicating the graphite-like nature of GNP. Notably, sharp reflections at $2\theta = 26.6°$ matching the (002) plane and at $2\theta = 54.7°$ matching the (004) plane were observed. These sharp reflections are indicative of the high crystallinity of GNP. XRD peaks of GNP nanoparticles indexed to the hexagonal crystal system GNP (P63/mmc space group, PDF 00-008-0415) [25]. Absence of impurities XRD peaks indicates that high quality of GNP nanoparticles was procured. The crystallite size of highest peak in XRD was 19.59 nm < 100nm. It suggested nanocrystalline characteristic of GNP nanoparticles. The lattice parameters of GNP nanoparticles are also reported in Table 3.3.

Table 3.3: The lattice parameters of GNP nanoparticles.

Nano-additive	**Lattice parameters**		**Full width at half maximum-FWHM (2θ) at peak 2θ=26.6°**	**Crystallite size by XRD (nm)**
	a	*c*		
Graphene nanoplatelets (GNP)	2.46	6.73	0.435°	19.59

Structure and morphological features of different samples were examined by SEM and the corresponding images are presented. Fig 3.10 shows GNP nanoparticles possess a distinctive platelet shape of less than 100 nm size. The composition of the GNP nano-additive was determined from different regions using EDX spectroscopy. The corresponding EDX spectra (Fig 3.11) peaks showed the presence of C. This suggests high purity of GNP nano-additives. The morphology and EDX analysis were in support of the XRD results which confirm the purity of GNP nano-additive.

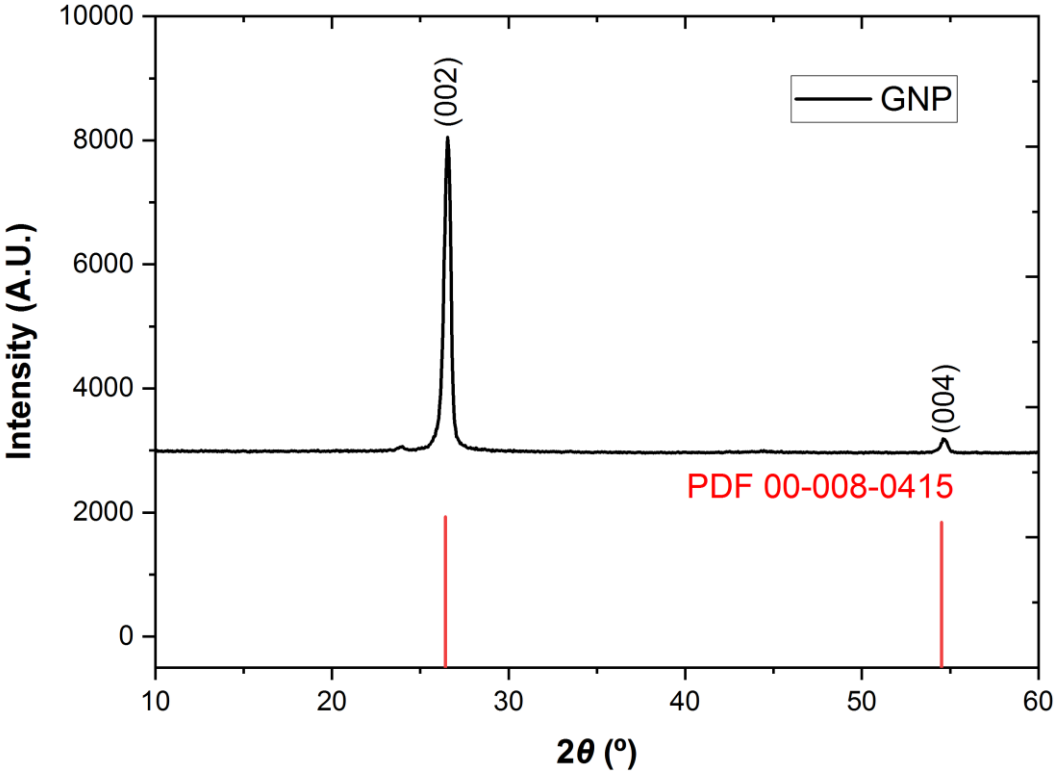

Fig. 3.9: XRD patterns of GNP.

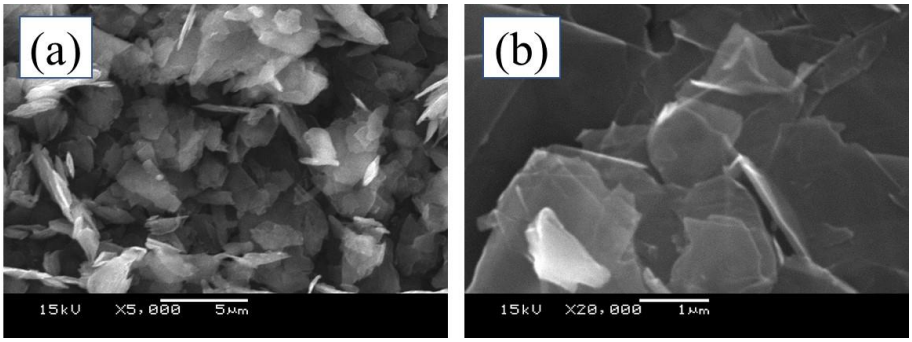

Fig. 3.10: SEM images of GNP.

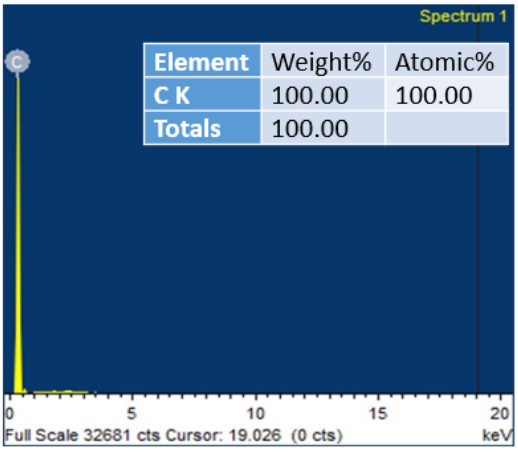

Fig. 3.11: EDX image of GNP.

3.4: Multiwalled carbon nanotubes (MWCNT)

Multiwalled carbon nanotubes (MWCNT) was acquired from Sigma-Aldrich (USA) and utilized without additional purification.

3.4.1: Characterization of MWCNT nanoparticles

The XRD graph of MWCNT nano-additives exhibits characteristic peaks (Fig. 3.12) indicating the graphite-like nature of MWCNT. Notably, sharp reflections at $2\theta = 26.1°$ matching (002) plane and at $2\theta = 42.7°$ matching (100) plane were observed. These sharp reflections are indicative of the high crystallinity of MWCNT. XRD peaks of MWCNT nanoparticles indexed to the hexagonal crystal system MWCNT (P63/mmc space group, PDF 00-008-0415) [25]. Absence of impurities XRD peaks indicates that high quality of MWCNT nanoparticles was procured. The crystallite size of highest peak in XRD was 9.92 nm < 100nm. It suggested nanocrystalline characteristic of MWCNT nanoparticles. The lattice parameters of MWCNT nanoparticles are also reported in Table 3.4.

Table 3.4: The lattice parameters of MWCNT nanoparticles.

Nano-additive	Lattice parameters		Full width at half maximum-FWHM (2θ) at peak 2θ=26.1°	Crystallite size by XRD (nm)
	a	*c*		
Multiwalled carbon nanotubes (MWCNT)	2.46	6.73	0.870°	9.92

Structure and morphological features of different MWCNT samples were examined by SEM and the corresponding images are presented. Fig 3.13 shows MWCNT nanoparticles possess a tube-shaped network of less than 100 nm size. The composition of the MWCNT nano-additive was determined from different regions using EDX spectroscopy. The corresponding EDX spectra (Fig 3.14) peaks showed the presence of C. This suggests high purity of MWCNT nano-additives. The morphology and EDX analysis were in support of the XRD results which confirm the purity of MWCNT nano-additive.

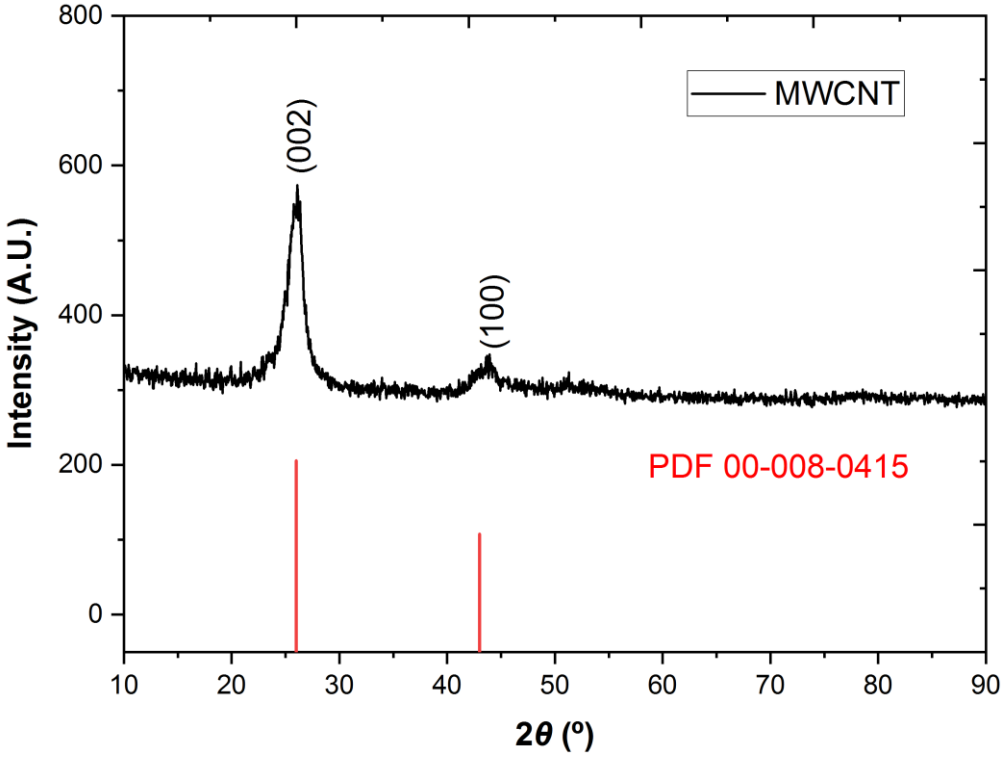

Fig. 3.12: XRD patterns of MWCNT.

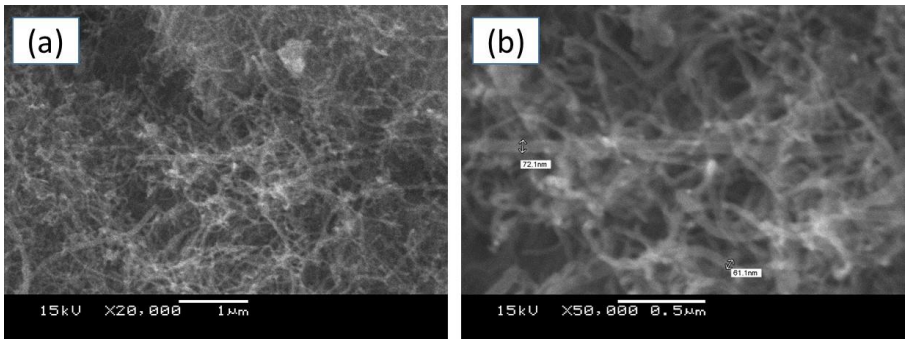

Fig. 3.13: SEM images of MWCNT.

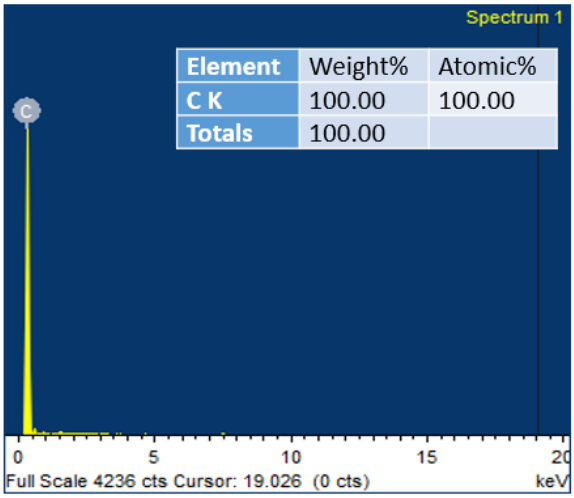

Fig. 3.14: EDX image of MWCNT.

3.5: References

[1] D. Xiang, L. Shen, and H. Wang, Investigation on the thermal conductivity of mineral oil-based alumina/aluminum nitride nanofluids, Materials, 12 (2019).

[2] G. Colangelo, E. Favale, P. Miglietta, M. Milanese, and A. de Risi, Thermal conductivity, viscosity and stability of Al_2O_3-diathermic oil nanofluids for solar energy systems, Energy, 95 (2016) 124-136.

[3] S. U. Ilyas, R. Pendyala, M. Narahari, and L. Susin, Stability, rheology and thermal analysis of functionalized alumina- thermal oil-based nanofluids for advanced cooling systems, Energy conversion and management, 142 (2017) 215-229.

[4] S. S. Sanukrishna, and M. Jose Prakash, Thermal and rheological characteristics of refrigerant compressor oil with alumina nanoparticles-An experimental investigation, Powder technology, 339 (2018) 119-129.

[5] K. Sepyani, M. Afrand, and M. Hemmat Esfe, An experimental evaluation of the effect of ZnO nanoparticles on the rheological behavior of engine oil, Journal of molecular liquids, 236 (2017) 198-204.

[6] L. Yang, M. Mao, J.-n. Huang, and W. Ji, Enhancing the thermal conductivity of SAE 50 engine oil by adding zinc oxide nano-powder: An experimental study, Powder technology, 356 (2019) 335-341.

[7] M. Hemmat Esfe, H. Rostamian, and M. Reza Sarlak, A novel study on rheological behavior of ZnO-MWCNT/10W40 nanofluid for automotive engines, Journal of molecular liquids, 254 (2018) 406-413.

[8] S. B. Mousavi, and S. Zeinali Heris, Experimental investigation of ZnO nanoparticles effects on thermophysical and tribological properties of diesel oil, International journal of hydrogen energy, 45 (2020) 23603-23614.

[9] M. Mehrali, E. Sadeghinezhad, S. T. Latibari, S. N. Kazi, M. Mehrali, M. N. B. M. Zubir, and H. S. C. Metselaar, Investigation of thermal conductivity and rheological properties of nanofluids containing graphene nanoplatelets, Nanoscale research letters, 9 (2014) 15.

[10] J. P. Vallejo, G. Żyła, J. Fernández-Seara, and L. Lugo, Rheological behaviour of functionalized graphene nanoplatelet nanofluids based on water and propylene glycol:water mixtures, International communications in heat and mass transfer, 99 (2018) 43-53.

[11] A. S. Al-Janabi, M. Hussin, and M. Z. Abdullah, Stability, thermal conductivity and rheological properties of graphene and MWCNT in nanolubricant using additive surfactants, Case studies in thermal engineering, 28 (2021) 101607.

[12] A. Naddaf, and S. Zeinali Heris, Experimental study on thermal conductivity and electrical conductivity of diesel oil-based nanofluids of graphene nanoplatelets and carbon nanotubes, International communications in heat and mass transfer, 95 (2018) 116-122.

[13] S. U. Ilyas, R. Pendyala, and M. Narahari, Stability and thermal analysis of MWCNT-thermal oil-based nanofluids, Colloids and Surfaces A: Physicochemical and engineering aspects, 527 (2017) 11-22.

[14] M.-S. Liu, M. Ching-Cheng Lin, I. T. Huang, and C.-C. Wang, Enhancement of thermal conductivity with carbon nanotube for nanofluids, International communications in heat and mass transfer, 32 (2005) 1202-1210.

[15] A. Beheshti, M. Shanbedi, and S. Z. Heris, Heat transfer and rheological properties of transformer oil-oxidized MWCNT nanofluid, Journal of thermal analysis and calorimetry, 118 (2014) 1451-1460.

[16] L. Chen, H. Xie, W. Yu, and Y. Li, Rheological behaviors of nanofluids containing multi-walled carbon nanotube, Journal of dispersion science and technology, 32 (2011) 550-554.

[17] V. Vora, R. K. Sharma, and D. P. Bharambe, Investigation of rheological and thermal conductivity properties of castor oil nanofluids containing graphene nanoplatelets, International journal of thermophysics, 44 (2023) 155.

[18] P. Ghosh, M. Hoque, and G. Karmakar, Castor oil as potential multifunctional additive in the formulation of eco-friendly lubricant, Polymer Bulletin, 75 (2018) 501-514.

[19] S. Senthilraja, M. Karthikeyan, and R. Gangadevi, Nanofluid applications in future automobiles: comprehensive review of existing data, Nano-Micro Letters, 2 (2010) 306-310.

[20] N. K. Bhoi, H. Singh, and S. Pratap, Synthesis and characterization of alumina nanoparticles: a case study, Journal of the Institution of Engineers (India): Series C, 101 (2020) 407-413.

[21] B. T. Polat, İ. E. Öner, S. Kan, K. Benzeşik, and O. Yücel, Fused calcium aluminate production from aluminum white dross residue, Journal of sustainable metallurgy, 8 (2022) 851-862.

[22] S. Fatimah, R. Ragadhita, D. F. Al Husaeni, and A. B. D. Nandiyanto, How to calculate crystallite size from x-ray diffraction (XRD) using Scherrer method, ASEAN Journal of Science and Engineering, 2 (2022) 65-76.

[23] T. Sahoo, M. Kim, J. H. Baek, S.-R. Jeon, J. S. Kim, Y.-T. Yu, C.-R. Lee, and I.-H. Lee, Synthesis and characterization of porous ZnO nanoparticles by hydrothermal treatment of as pure aqueous precursor, Materials Research Bulletin, 46 (2011) 525-530.

[24] A. S. Mokrushin, I. A. Nagornov, A. A. Averin, N. P. Simonenko, T. L. Simonenko, E. P. Simonenko, V. G. Sevastyanov, and N. T. Kuznetsov, Effect of the addition of cerium acetylacetonate on the synthesis of ZnO nanopowder, Russian Journal of Inorganic Chemistry, 66 (2021) 638-644.

[25] O. L. Li, S. Chiba, Y. Wada, G. Panomsuwan, and T. Ishizaki, Synthesis of graphitic-N and amino-N in nitrogen-doped carbon via a solution plasma process and exploration of their synergic effect for advanced oxygen reduction reaction, Journal of materials chemistry A, 5 (2017) 2073-2082.